Mineralogical Magazine (2023), **87**, 79–85
doi:10.1180/mgm.2022.117

CAMBRIDGE UNIVERSITY PRESS

Article

Loomisite, $Ba[Be_2P_2O_8]\cdot H_2O$, the first natural example with the zeolite ABW-type framework, from Keystone, Pennington County, South Dakota, USA

Hexiong Yang[1]*, Xiangping Gu[2], Ronald B. Gibbs[1] and Robert T. Downs[1]

[1]Department of Geosciences, University of Arizona, 1040 E. 4th Street, Tucson, AZ 85721-0077, USA; and [2]School of Geosciences and Info-Physics, Central South University, Changsha, Hunan 410083, China

Abstract

A new beryllophosphate mineral species, loomisite (IMA2022-003), ideally $Ba[Be_2P_2O_8]\cdot H_2O$, was found from the Big Chief mine near Keystone, Pennington County, South Dakota, USA. It occurs as divergent sprays of very thin bladed crystals with a tapered termination. Individual crystals are found up to 0.80 × 0.06 × 0.03 mm. Associated minerals include dondoellite, earlshannonite, mitridatite, rockbridgeite, jahnsite-(CaMnFe) and quartz. No twinning or parting is observed macroscopically. Loomisite is murky white in transmitted light, transparent with white streak and silky to vitreous lustre. It is brittle and has a Mohs hardness of 3½–4, with perfect cleavage on {100} and {$\bar{1}$10}. The measured and calculated densities are 3.46(5) and 3.512 g/cm^3, respectively. Optically, loomisite is biaxial (+), with $\alpha = 1.579(5)$, $\beta = 1.591(5)$, $\gamma = 1.606(5)$ (white light), 2V (meas.) = 82(2)° and 2V (calc.) = 85°. It is non-pleochroic under polarised light, with a very weak ($r > v$) dispersion. The mineral is insoluble in water or hydrochloric acid. An electron microprobe analysis, along with the BeO content measured with an ICP-MS, yields an empirical formula (based on 9 O apfu) $(Ba_{0.96}Ca_{0.06})_{\Sigma 1.02}[(Be_{1.96}Fe_{0.06})_{\Sigma 2.02}P_{1.99}O_8]\cdot H_2O$, which can be simplified to $(Ba,Ca)[(Be,Fe)_2P_2O_8]\cdot H_2O$.

Loomisite is monoclinic, with space group *Pn* and unit-cell parameters $a = 7.6292(18)$, $b = 9.429(2)$, $c = 4.7621(11)$ Å, $\beta = 91.272(5)°$, $V = 342.47(14)$ Å^3 and $Z = 2$. Its crystal structure is characterised by a framework of corner-sharing PO_4 and BeO_4 tetrahedra. The framework can be considered as built from the stacking of sheets consisting of 4- and 8-membered rings (4.8^2 nets) along [001] or hexagonal layers (6^3 nets) along [010]. The extra-framework Ba^{2+} and H_2O are situated in the channels formed by the 8-membered rings. Topologically, loomisite represents the first natural example with the zeolite **ABW**-type framework, which is adopted by over 100 synthetic compounds with different chemical compositions.

Keywords: loomisite, beryllophosphate, zeolite, **ABW**-type framework, new mineral, crystal structure, X-ray diffraction

(Received 4 September 2022; accepted 4 October 2022; Accepted Manuscript published online: 20 October 2022; Associate Editor: G. Diego Gatta)

Introduction

A new beryllophosphate mineral species, loomisite, ideally $Ba[Be_2P_2O_8]\cdot H_2O$, was found on specimens collected from the Big Chief mine near Keystone, Pennington County, South Dakota, USA. It is named in honour of Mr. Thomas A. Loomis, the owner of Dakota Matrix Minerals, Inc., who has generously donated/provided over 200 mineral specimens, known or unknown, including the loomisite specimen, to the RRUFF Project (http://rruff.info) for research and data collection. Thomas received his B.S. degree in Geological Engineering from the South Dakota School of Mines and has field-collected and studied minerals from the Black Hills, South Dakota since 1978. The new mineral and its name (symbol Lmi) have been approved by the Commission on New Minerals, Nomenclature and Classification (CNMNC) of the International Mineralogical Association (IMA2022-003, Yang *et al.*, 2022). The cotype samples have been deposited at the University of Arizona Alfie Norville Gem and Mineral Museum (Catalogue # 22725) and the RRUFF Project (deposition # R210017) (http://rruff.info).

Although beryllophosphate minerals are relatively rare in Nature (less than three dozen to date), they are of great interest because their structures are similar to those of aluminosilicates and borosilicates and exhibit a variety of structure types due to different polymerisation of the BeO_4–PO_4 tetrahedra, including clustered, chain, sheet, framework and zeolite-type structures (e.g. Kampf 1992; Hawthorne and Huminicki 2002; Dal Bo *et al.*, 2014). Thus far, several framework beryllophosphate minerals have been reported, such as tiptopite with the sodalite-type framework, $K_2(Li,Na,Ca)_6(Be_6P_6)O_{24}(OH)_2\cdot 1.3H_2O$ (Grice *et al.*, 1985), pahasapaite with the zeolite **RHO**-type framework, $Li_8(Ca,Li,K)_{10}Be_{24}(PO_4)_{24}\cdot 38H_2O$ (Rouse *et al.*, 1987), and limousinite, $BaCa[Be_4P_4O_{16}]\cdot 6H_2O$ and wilancookite, $(Ba_5Li_2\square)Ba_6Be_{24}P_{24}O_{96}\cdot 26H_2O$, with the phillipsite-type framework (Hatert *et al.*, 2020). Loomisite is the first natural example with the zeolite **ABW**-type framework, which is adopted by over 100 synthetic compounds with different chemical compositions (e.g.

*Author for correspondence: Hexiong Yang, Email: hyang@arizona.edu
Cite this article: Yang H., Gu X., Gibbs R.B. and Downs R.T. (2023) Loomisite, $Ba[Be_2P_2O_8]\cdot H_2O$, the first natural example with the zeolite ABW-type framework, from Keystone, Pennington County, South Dakota, USA. *Mineralogical Magazine* **87**, 79–85. https://doi.org/10.1180/mgm.2022.117

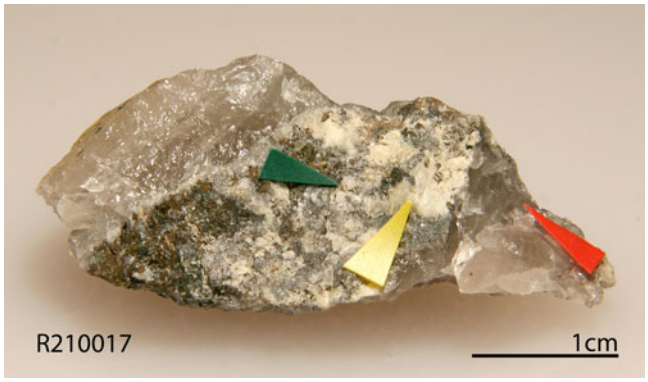

Fig. 1. The specimen (R210017) on which the new mineral loomisite was found.

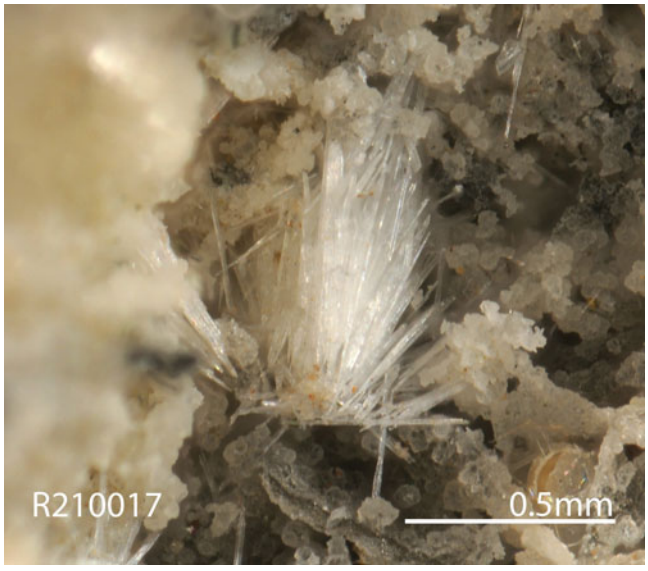

Fig. 2. A microscopic view of a sprays of white, very thin bladed loomisite crystals (R210017).

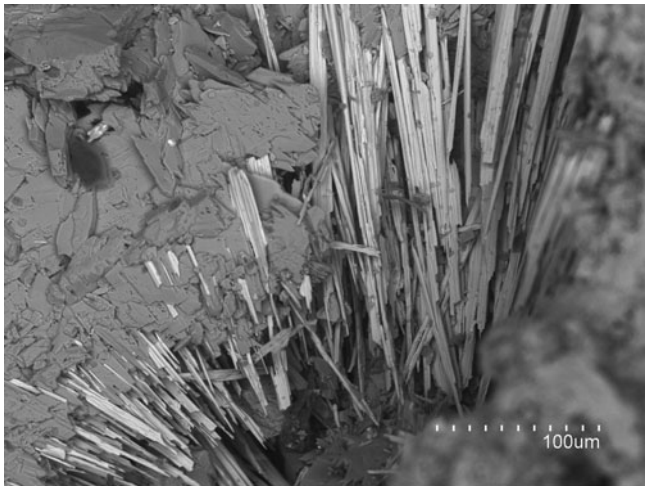

Fig. 3. A back-scattered electron image of thin bladed loomisite crystals (R210017). The matrix is primarily dondoellite.

Table 1. Chemical compositions (in wt.%) for loomisite.

Constituent	Mean	Range	S.D.	Probe standard
P_2O_5	38.66	38.24–39.13	0.33	Synthetic apatite
CaO	0.85	0.49–1.28	0.22	Synthetic apatite
FeO	1.12	0.77–1.52	0.17	Fayalite
BaO	40.17	39.57–40.64	0.28	Barite
BeO*	13.39			ICP-MS
H_2O**	4.94			
Total	99.13	98.51–99.86	0.59	

*The BeO content was measured with an X-Series 2 quadrupole ICP-MS.
**The H_2O content was added according to the ideal value of H_2O.
S.D. – standard deviation

Bu *et al.*, 1997; Kahlenberg *et al.*, 2001). This paper describes the physical and chemical properties of loomisite and its crystal structure determined from single-crystal X-ray diffraction data, illustrating its structural relationships with zeolite-type frameworks.

Sample description and experimental methods

Occurrence, physical and chemical properties, and Raman spectra

Loomisite was found on specimens (Fig. 1) collected from the Big Chief mine (43°51'54"N, 103°22'54"W), near Keystone, Pennington County, South Dakota, USA. Associated minerals on the type sample include dondoellite $Ca_2Fe(PO_4)_2{\cdot}2H_2O$, earlshannonite $Mn^{2+}Fe_2^{3+}(PO_4)_2(OH)_2{\cdot}4H_2O$, mitridatite $Ca_2Fe_3^{3+}O_2(PO_4)_3{\cdot}3H_2O$, rockbridgeite $(Fe_{0.5}^{2+}Fe_{0.5}^{3+})_2Fe_3^{3+}(PO_4)_3(OH)_5$, jahnsite-(CaMnFe) $CaMn^{2+}Fe_2^{2+}Fe_2^{3+}(PO_4)_4(OH)_2{\cdot}8H_2O$, and quartz. On a larger scale, loomisite was found in a boulder containing ludlamite $Fe_3^{2+}(PO_4)_2{\cdot}4H_2O$, vivianite $Fe_3^{2+}(PO_4)_2{\cdot}8H_2O$, and, to a lesser extent, phosphoferrite $Fe_3^{2+}(PO_4)_2{\cdot}3H_2O$, perloffite $BaMn_2^{2+}Fe_2^{3+}(PO_4)_3(OH)_3$, and kryzhanovskite $(Fe^{3+},Mn^{2+})_3(PO_4)_2(OH,H_2O)_3$. The Big Chief pegmatite was mined for feldspar in the 1930s. Its geology and mineralogy were reported by Norton (1964), Roberts and Rapp (1965), and Campbell and Roberts (1985). Primary iron-manganese phosphates and beryl were chemically attacked, producing secondary phosphates such as loomisite and those mentioned above. The Big Chief pegmatite is the type locality for metavivianite (Ritz *et al.*, 1974), olmsteadite (Moore *et al.*, 1976) and perloffite (Kampf, 1977).

Loomisite occurs as divergent sprays of very thin bladed crystals that gently taper to a blunt termination. Individual crystals are found up to 0.80 × 0.06 × 0.03 mm (Figs 2 and 3). No twinning or parting is observed macroscopically. The mineral is murky white in transmitted light, transparent with white streak and silky to vitreous lustre. It is brittle and has a Mohs hardness of 3½–4, with perfect cleavage on {100} and {$\bar{1}$10}. The density measured by flotation in heavy liquids is 3.46(5) g/cm^3 and the calculated density is 3.512 g/cm^3. Optically, loomisite is biaxial (+), with $\alpha = 1.579(5)$, $\beta = 1.591(5)$, $\gamma = 1.606(5)$ (white light), 2V (meas.) = 82(2)° and 2V (calc.) = 85°. It is non-pleochroic under polarised light and the dispersion is very weak with $r > v$. The calculated compatibility index based on the empirical formula is 0.045 (good) (Mandarino, 1981). Loomisite is insoluble in water or hydrochloric acid.

The chemical composition of loomisite was determined using a Cameca SX-100 electron microprobe (WDS mode, 15 kV, 10 nA and a beam diameter of 5 μm). The standards used for the probe analysis are given in Table 1, along with the determined compositions (5 analysis points) and the BeO content measured with an X-Series 2 quadrupole ICP-MS following the procedure described

https://doi.org/10.1180/mgm.2022.117 Published online by Cambridge University Press

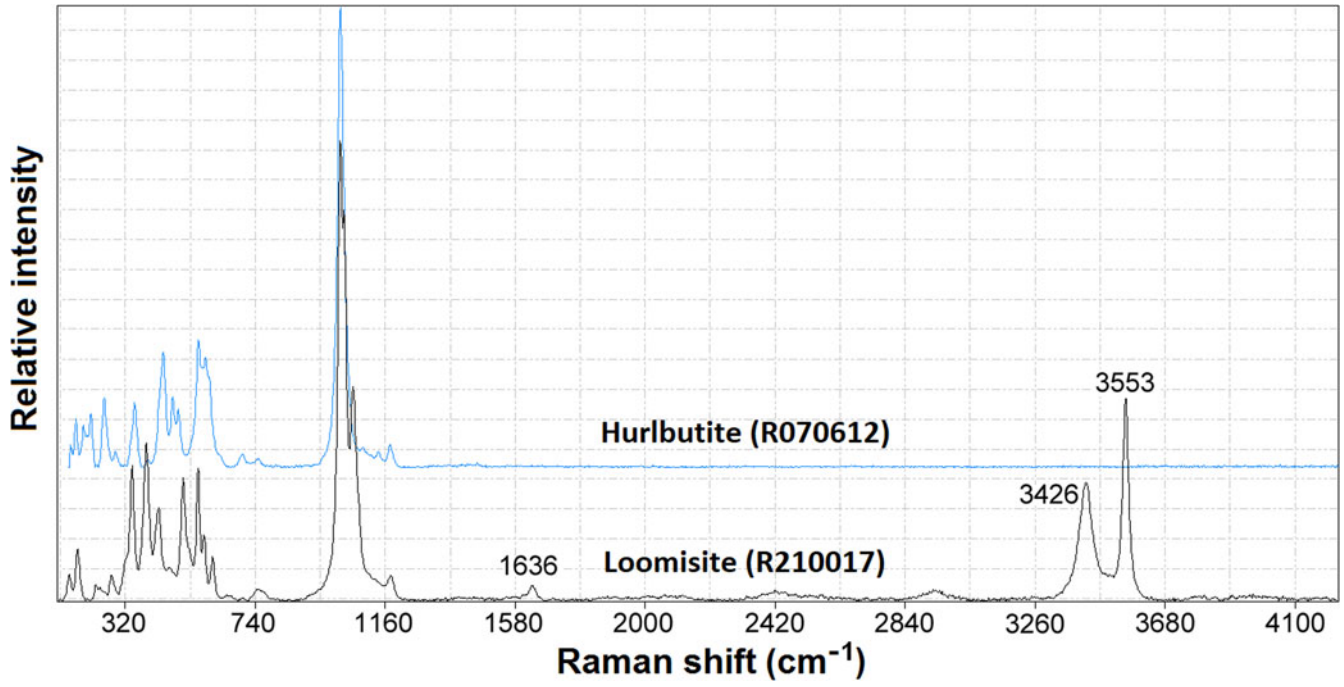

Fig. 4. Raman spectra of loomisite and hurlbutite, $CaBe_2(PO_4)_2$.

Table 2. Powder X-ray diffraction data (*d* in Å, *I* in %) for loomisite.

I_{cal}	I_{meas}	d_{cal}	d_{meas}	*h k l*	I_{cal}	I_{meas}	d_{cal}	d_{meas}	*h k l*
66.5	**27.2**	**5.941**	**5.945**	**1 1 0**	4.1	9.7	1.755	1.757	0 5 1
13.9	5.9	4.721	4.741	0 2 0	3.4	15.7	1.732	1.731	3 4 0
65.7	**38.9**	**4.248**	**4.259**	**0 1 1**	1.9	1.1	1.714	1.710	$\bar{1}$ 5 1
13.8	8.8	4.077	4.096	1 0 $\bar{1}$	5.4	7.9	1.693	1.695	3 1 2
2.7	19.9	4.017	4.033	1 2 0	5.4	7.5	1.675	1.677	0 4 2
40.5	29.2	3.822	3.813	2 0 0	8.4	12.0	1.635	1.636	$\bar{3}$ 4 1
9.9	7.5	3.743	3.723	$\bar{1}$ 1 1	7.4	9.4	1.620	1.621	3 4 1
9.8	5.0	3.684	3.667	1 1 1	4.8	4.9	1.600	1.597	$\bar{2}$ 5 1
11.2	8.1	3.543	3.548	2 1 0	7.8	20.7	1.574	1.574	0 6 0
12.8	8.2	3.351	3.353	0 2 1	2.8	0.9	1.553	1.552	$\bar{4}$ 3 1
35.6	**44.5**	**3.086**	**3.068**	**$\bar{1}$ 2 1**	4.8	3.0	1.534	1.535	$\bar{3}$ 3 2
17.9	12.5	2.971	2.970	2 2 0	3.5	13.1	1.509	1.509	5 1 0
100.0	**100.0**	**2.910**	**2.897**	**1 3 0**	3.2	10.8	1.485	1.484	4 4 0
67.6	**65.1**	**2.868**	**2.869**	**$\bar{2}$ 1 1**	2.2	9.7	1.475	1.472	4 0 2
46.3	**54.0**	**2.815**	**2.816**	**2 1 1**	3.6	16.9	1.469	1.461	1 2 3
17.0	16.1	2.625	2.628	0 3 1	5.0	16.4	1.437	1.438	2 1 3
2.4	0.9	2.538	2.547	$\bar{2}$ 2 1	2.6	2.6	1.416	1.418	0 3 3
17.3	23.7	2.460	2.460	3 1 0	7.1	24.3	1.375	1.376	5 3 0
36.6	**57.8**	**2.378**	**2.385**	**0 0 2**	4.5	6.1	1.312	1.311	0 6 2
8.4	12.8	2.266	2.268	3 0 $\bar{1}$	2.8	1.7	1.298	1.299	$\bar{4}$ 5 1
6.9	15.2	2.220	2.223	$\bar{1}$ 1 2	4.8	10.5	1.283	1.285	3 2 3
13.1	20.5	2.196	2.191	1 1 2	2.1	5.5	1.272	1.274	3 5 2
20.8	26.9	2.152	2.152	2 3 1	1.8	2.4	1.269	1.263	$\bar{4}$ 4 2
12.4	23.1	2.124	2.126	0 2 2	1.8	2.0	1.246	1.248	$\bar{2}$ 6 2
13.0	34.7	2.043	2.045	$\bar{1}$ 4 1	3.0	6.2	1.231	1.231	$\bar{2}$ 7 1
18.9	26.6	2.014	2.012	3 2 1	1.6	5.6	1.214	1.215	0 5 3
8.6	13.4	1.980	1.980	3 3 0	3.4	6.8	1.200	1.202	$\bar{5}$ 3 2
2.4	2.7	1.957	1.958	2 1 2					
6.0	16.3	1.911	1.912	4 0 0					
6.4	8.5	1.871	1.877	$\bar{2}$ 2 2					
12.0	25.2	1.849	1.845	$\bar{1}$ 3 2					
11.2	20.1	1.834	1.834	1 3 2					
5.9	12.8	1.771	1.772	4 2 0					

The strongest lines are given in bold.

https://doi.org/10.1180/mgm.2022.117 Published online by Cambridge University Press

Table 3. Summary of crystallographic data and refinement results for loomisite.

Crystal data	
Ideal formula	$Ba[Be_2P_2O_8]\cdot H_2O$
Crystal symmetry	Monoclinic
Space group	*Pn*
a (Å)	7.6292(18)
b (Å)	9.429(2)
c (Å)	4.7621(11)
β (°)	91.272(5)
V (Å^3)	342.47(14)
Z	2
ρ_{cal} (g/cm^3)	3.476
Data collection	
Diffractometer	Bruker-APEX2
X-ray radiation	Mo*K*α (λ = 0.71073)
Temperature	293(2)
F(000)	332
2θ range for data collection (°)	≤66.08
No. of reflections collected	7602
No. of independent reflections	1289
No. of reflections with $I > 2\sigma(I)$	1077
R_{int}	0.051
Refinement	
Refinement method	Multi-scan
No. of parameters refined	128
Final R_1, wR_2 factors [$I > 2\sigma(I)$]	0.056, 0.091
Goodness-of-fit	1.097

Table 6. Selected bond distances for loomisite.

P1–O1	1.539(13)	P2–O5	1.521(10)
P1–O2	1.543(11)	P2–O6	1.532(9)
P1–O3	1.543(9)	P2–O7	1.557(8)
P1–O4	1.517(10)	P2–O8	1.542(10)
<P1–O>	1.535	<P2–O>	1.538
Be1–O2	1.624(18)	Be2–O1	1.62(2)
Be1–O3	1.62(2)	Be2–O6	1.60(2)
Be1–O4	1.59(2)	Be2–O7	1.58(2)
Be1–O5	1.63(2)	Be2–O8	1.651(17)
<Be1–O>	1.617	<Be2–O>	1.612
Ba–O9	2.744(14)		
Ba–O9	2.786(11)		
Ba–O6	2.818(8)		
Ba–O7	2.832(9)		
Ba–O1	2.839(12)		
Ba–O8	2.843(9)		
Ba–O4	2.931(10)		
Ba–O5	3.115(10)		
Ba–O2	3.200(10)		
Ba–O1	3.214(10)		
Ba–O6	3.281(8)		
<Ba–O>^{7}	2.828		
<Ba–O>^{11}	2.964		

Table 4. Fractional atomic coordinates and equivalent isotropic displacement parameters (Å^2) for loomisite.

Atom	*x*	*y*	*z*	U_{eq}
Ba*	0.88736(17)	0.73834(8)	0.56787(18)	0.0126(2)
Ca*	0.88736(17)	0.73834(8)	0.56787(18)	0.0126(2)
Be1	0.437(3)	0.879(2)	0.620(3)	0.008(3)
Be2	0.163(2)	0.615(2)	1.090(3)	0.010(3)
P1	0.2266(5)	0.9175(3)	0.1038(6)	0.0072(7)
P2	0.3688(6)	0.5773(3)	0.6090(6)	0.0079(8)
O1	0.1257(16)	0.7811(13)	0.026(2)	0.010(2)
O2	0.3982(13)	0.9287(11)	−0.0602(16)	0.014(2)
O3	0.2698(13)	0.9183(10)	0.4218(17)	0.013(2)
O4	0.1131(13)	1.0445(10)	0.0274(17)	0.012(2)
O5	0.4815(13)	0.7101(9)	0.600(2)	0.0135(19)
O6	0.4751(12)	0.4498(9)	0.5087(16)	0.0080(17)
O7	0.3150(14)	0.5465(10)	0.9165(16)	0.014(2)
O8	0.1985(12)	0.5904(10)	0.4299(16)	0.0082(17)
O9	0.7079(19)	0.7725(15)	1.067(3)	0.019(3)

*Occupancies <1: Ba 0.950(12), Ca 0.052(12)

by Xing *et al.* (2021). The resultant chemical formula, calculated on the basis of 9 O atoms per formula unit (from the structure determination), is $(Ba_{0.96}Ca_{0.06})_{\Sigma 1.02}[(Be_{1.96}Fe_{0.06})_{\Sigma 2.02}P_{1.99}O_8]\cdot H_2O$, which can be simplified to $(Ba,Ca)[(Be,Fe)_2P_2O_8]\cdot H_2O$.

The Raman spectrum of loomisite (Fig. 4) was collected on a randomly oriented crystal with a Thermo Almega microRaman system, using a solid-state laser with a wavelength of 532 nm at the full power of 150 mW and a thermoelectric cooled CCD detector. The laser is partially polarised with 4 cm^{-1} resolution and a spot size of 1 μm.

X-ray crystallography

The powder X-ray diffraction data of loomisite (Table 2) were collected on a Rigaku Xtalab Synergy single crystal diffractometer (Cu*K*α radiation) in Gandolfi powder mode at 50 kV and 1 mA. The unit-cell parameters refined using the program by Holland and Redfern (1997) are as follows: $a = 7.6457(2)$, $b = 9.4427(3)$, $c = 4.7512(2)$ Å, $\beta = 91.272(5)°$, and $V = 342.47(14)$ Å^3.

Table 5. Atomic displacement parameters (Å^2) for loomisite.

Atom	U^{11}	U^{22}	U^{33}	U^{12}	U^{13}	U^{23}
Ba	0.0148(4)	0.0131(4)	0.0098(2)	0.0045(7)	−0.00153(18)	−0.0002(5)
Be1	0.007(9)	0.009(8)	0.010(6)	0.006(7)	−0.001(5)	0.000(5)
Be2	0.003(9)	0.018(9)	0.008(5)	−0.004(7)	0.000(5)	0.002(6)
P1	0.0078(18)	0.0071(16)	0.0069(11)	−0.0015(12)	0.0007(10)	0.0005(9)
P2	0.010(2)	0.0073(15)	0.0062(15)	0.0016(14)	0.0005(12)	−0.0002(9)
O1	0.011(7)	0.009(5)	0.010(4)	0.001(4)	0.000(4)	0.005(3)
O2	0.011(5)	0.020(5)	0.010(3)	0.012(4)	−0.006(3)	−0.003(3)
O3	0.013(5)	0.015(5)	0.010(3)	0.010(4)	−0.004(3)	0.000(3)
O4	0.019(6)	0.005(4)	0.013(4)	0.003(4)	0.004(3)	0.001(3)
O5	0.010(5)	0.005(5)	0.026(4)	0.000(4)	0.004(4)	−0.001(3)
O6	0.005(5)	0.007(4)	0.012(3)	0.002(3)	0.004(3)	−0.004(3)
O7	0.022(6)	0.013(5)	0.006(3)	0.008(4)	0.000(3)	0.006(3)
O8	0.006(5)	0.009(4)	0.009(3)	−0.001(4)	0.001(3)	0.000(3)
O9	0.020(8)	0.027(7)	0.011(4)	0.011(6)	0.005(4)	−0.008(4)

https://doi.org/10.1180/mgm.2022.117 Published online by Cambridge University Press

Table 7. Bond-valence sums for loomisite.

	Ba	Be1	Be2	P1	P2	Σ
O1	0.224		0.521	1.278		2.104
	0.081					
O2	0.084	0.518		1.266		1.868
O3		0.531		1.266		1.796
O4	0.174	0.565		1.357		2.096
O5	0.106	0.504			1.343	1.953
O6	0.237		0.560		1.302	2.168
	0.068					
O7	0.228		0.588		1.218	2.034
O8	0.221		0.482		1.267	1.970
O9	0.289					0.574
	0.258					
Σ	1.971	2.117	2.151	5.167	5.130	

All loomisite crystals examined are pervasively twinned on (100) with the twin law [1 0 0 / 0 $\bar{1}$ 0 / 0 0 $\bar{1}$] or consist of multi-crystal intergrowth, making it very difficult to find a suitable single crystal for X-ray intensity data collection. The X-ray intensity data used for the structure analysis were collected from a bladed fragment with the size of 0.06 × 0.02 × 0.01 mm on a Bruker APEX2 CCD X-ray diffractometer equipped with graphite-monochromatised Mo*K*α radiation with frame widths of 0.5° in ω and 30 s counting time per frame. The intensity data were processed using the Bruker *TWINABS* software, yielding a twin ratio of 59:41. The systematic absences of reflections suggest possible space group *P*2/*n*, *Pn*, or *P*2. The crystal structure was solved and refined using *SHELX2018* (Sheldrick 2015a, 2015b) based on space group *Pn*, because it produced the better refinement statistics in terms of bond lengths and angles, atomic displacement parameters, and *R* factors. No H atoms were located through the difference-Fourier syntheses. Refinement statistics are given in Table 3. Final atomic coordinates and displacement parameters are given in Tables 4 and 5, respectively. Selected bond distances are presented in Table 6. The bond-valence sums were calculated using the parameters given by Brese and O'Keefe (1991) (Table 7). The crystallographic information file has been deposited with the Principal Editor of *Mineralogical Magazine* and is available as Supplementary material (see below).

Crystal structure description and discussion

The crystal structure of loomisite is characterised by a framework of corner-sharing PO_4 and BeO_4 tetrahedra, with a topology identical to that of the zeolite **ABW** type (e.g. Bu *et al.*, 1997; Kahlenberg *et al.*, 2001). The framework can be considered as built from the stacking of sheets consisting of 4- and 8-membered rings (4.8^2 nets) along [001] (Fig. 5) or hexagonal layers (6^3 nets) along [010] (Fig. 6). The extra-framework Ba^{2+} and H_2O are situated in the channels formed by the 8-membered rings. For comparison, Figs 5 and 6 also show the structure for the **ABW**-type $M^+[BePO_4]$ compounds with space group $Pna2_1$ (M^+ = Li, K, Rb and NH_4) (e.g. Bu *et al.*, 1997; Zhang *et al.*, 2001). As in other framework beryllophosphates, every framework O atom in loomisite is bonded to one P and one Be, giving rise to an ordered arrangement of P and Be atoms in the framework. Any linkages of P–O–P or Be–O–Be are strictly forbidden because they would make bridging O atoms either over-bonded or under-bonded (e.g. Hatert *et al.*, 2020 and references therein).

All average <P–O> and <Be–O> bond lengths in loomisite are comparable to those in other beryllophosphate minerals (e.g.

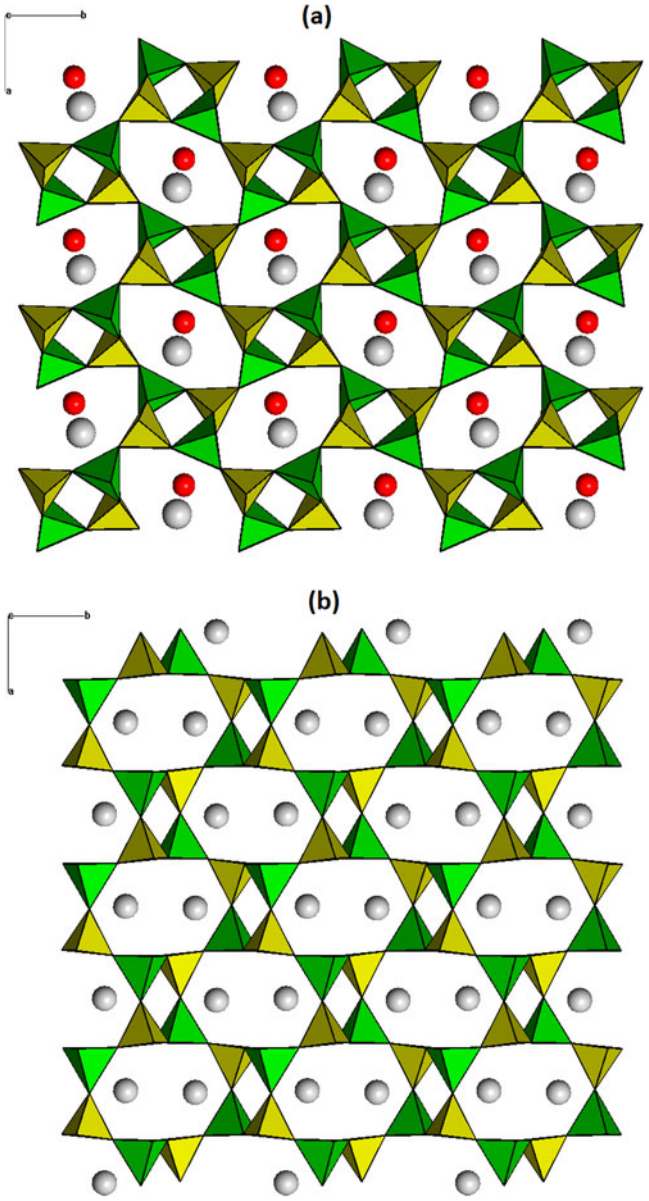

Fig. 5. (a) The crystal structure of loomisite, viewed as the stacking of sheets consisting of 4- and 8-membered PO_4 and BeO_4 tetrahedral rings (4.8^2 nets) along [001]. The extra-framework Ba^{2+} (grey spheres) and H_2O (red spheres) are situated in the channels formed by the 8-membered rings. The yellow and green tetrahedra represent PO_4 and BeO_4 groups, respectively. (b) The structure for the **ABW**-type $M^+[BePO_4]$ compounds with the space group $Pna2_1$ (M^+ = Li, K, Rb and NH_4) (e.g. Bu *et al.*, 1997; Zhang *et al.*, 2001). The M^+ cations are represented by grey spheres.

Grice *et al.*, 1985; Rouse *et al.*, 1987; Hatert *et al.*, 2020). The Ba^{2+} cation in the big cavity shows a (7+4) coordination, with seven Ba–O distances between 2.74 and 2.94 Å, and four between 3.11 and 3.30 Å (Table 6).

Although we were unable to locate H atoms from the structure refinement, a calculation of the O–O distances around the O9 atom (H_2O) in the cavity shows that eight O atoms are within 3.2 Å, which may be divided into two groups. Group 1 includes O2, O4, O5 and O6, which are at distances between 2.84 and 2.94 Å from O9, whereas group 2 includes O1, O3, O4 and O5, which are at distances between 3.04 and 3.20 Å from O9, as illustrated in Fig. 7. This observation suggests that H_2O in loomisite might form dynamic, rather than static, H-bonds with these 8 O atoms.

https://doi.org/10.1180/mgm.2022.117 Published online by Cambridge University Press

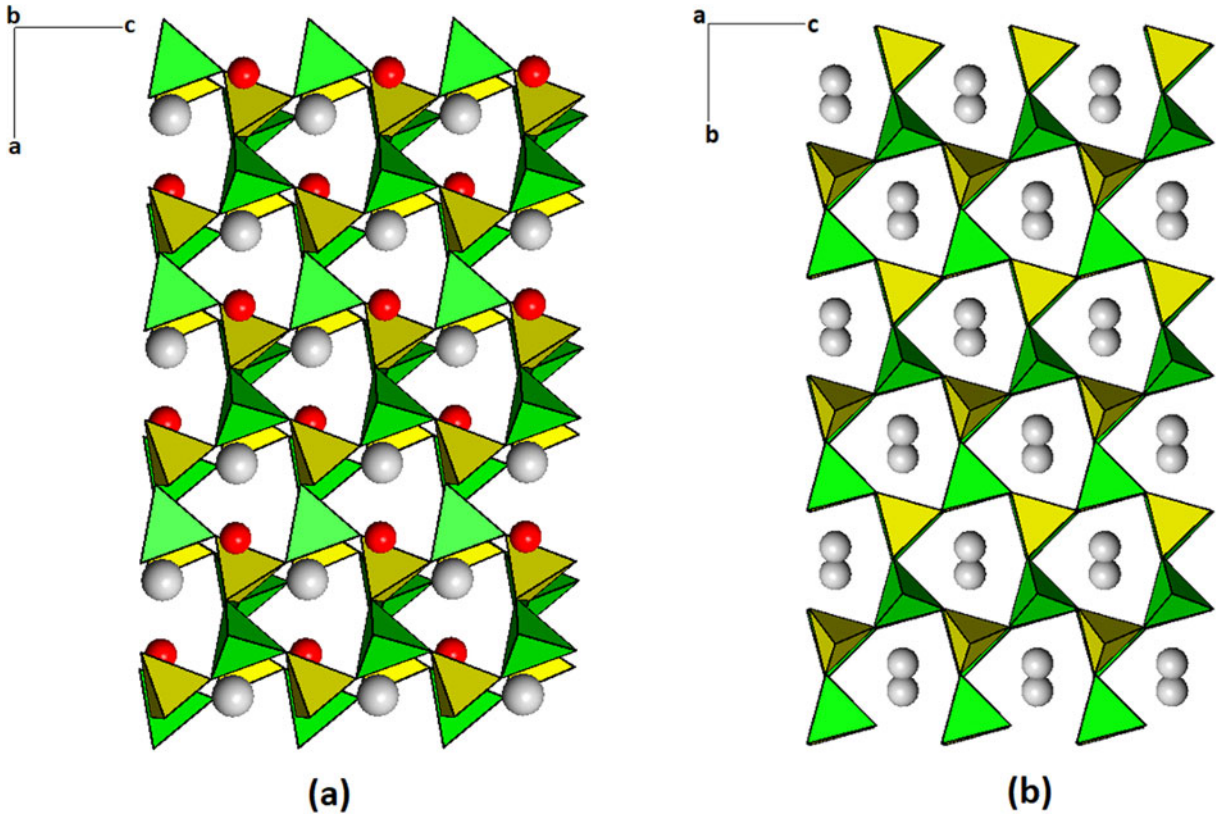

Fig. 6. Crystal structure of (a) loomisite and (b) the **ABW**-type zeolite, showing the stacking of hexagonal layers (6^3 nets) along [010] for loomisite and along [100] for the **ABW**-type zeolite. All figure legends are the same as in Fig. 4.

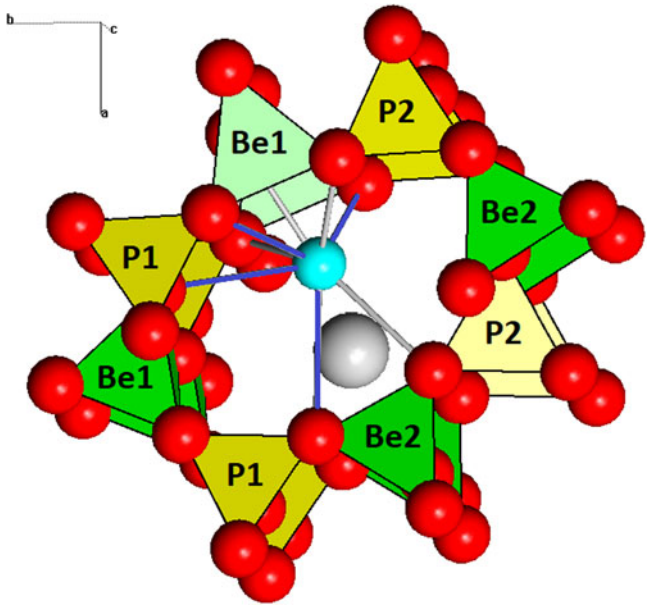

Fig. 7. An illustration of possible H-bonds for H_2O in an 8-membered tetrahedral ring. The red, grey, and aqua spheres represent O, Ba and H_2O, respectively. Four grey lines are for the O–O distances between 2.84–2.94 Å and four blue ones between 3.04–3.20 Å.

Based on previous Raman spectroscopic studies on beryllophosphate minerals (e.g. Frost *et al.*, 2012, 2014; Gatta *et al.*, 2014), we made the following tentative assignments of major Raman bands for loomisite. The two relatively strong bands centred at 3426 and 3553 cm^{-1} are assigned to the O–H stretching vibrational and a weak band centred at 1636 cm^{-1} to the H–O–H bending vibration in H_2O. The nature of the two weak and broad bands at 2437 and 2938 cm^{-1} are unclear. The bands between 720 and 1150 cm^{-1} are ascribable to the P–O and Be–O stretching vibrations within the PO_4 and BeO_4 groups, whereas those from 400 to 660 cm^{-1} are due to the O–P–O and O–Be–O bending vibrations. The bands below 400 cm^{-1} are mainly associated with the rotational and translational modes of PO_4 and BeO_4 tetrahedra, Ba–O stretching, and lattice vibrational modes. According to the correlation between ν_{O-H} and O—H···O distances for minerals (Libowitzky,1999), the Raman band at 3426 cm^{-1} corresponds well with the O–O distances of 2.84–2.94 Å and that at 3553 cm^{-1} with the O–O distances of 3.04–3.20 Å. Because hurlbutite, $CaBe_2(PO_4)_2$, also possesses a framework structure similar to that of loomisite (see below), its Raman spectrum from the RRUFF Project (http://rruff.info/R070612) is also plotted in Fig. 4 for comparison. Except for the region above 1200 cm^{-1}, the strong resemblance between the two spectra is apparent. The difference in peak intensities between the two spectra principally results from the different crystal orientations when the data were collected.

Loomisite is the first natural example with the zeolite **ABW**-type framework and the fifth natural Ba-beryllophosphate known to date, after babefphite $BaBe(PO_4)F$, minjiangite $BaBe_2(PO_4)_2$, wilancookite $(Ba_5Li_2\square)Ba_6Be_{24}P_{24}O_{96}\cdot 26H_2O$, and limousinite $BaCa[Be_4P_4O_{16}]\cdot 6H_2O$. According to Bu *et al.* (1997) and Kahlenberg *et al.* (2001), six different symmetries have been reported for the structures with the **ABW**-type framework, including *Imam*, *Pnam*, $Pna2_1$, $P2_1/c$ (or $P2_1/a$ or $P2_1/n$),

https://doi.org/10.1180/mgm.2022.117 Published online by Cambridge University Press

$P2_1$, $P\bar{1}$, with $Pna2_1$ and $P2_1$ being the most common space groups at room temperature. Loomisite represents the first **ABW**-type structure with space group *Pn*, expanding the diversity of the **ABW**-type framework symmetries.

In addition to babefphite $BaBe(PO_4)F$ and minjiangite $BaBe_2(PO_4)_2$, hurlbutite $CaBe_2(PO_4)_2$ and hydroxylherderite $CaBe(PO_4)(OH)$ are also related to loomisite in terms of chemical compositions. Among these minerals, hurlbutite also exhibits a framework consisting of 4-, 6-, and 8-membered rings (Lindbloom *et al.*, 1974; Dal Bo *et al.*, 2014), analogous to that of danburite, but its linkage between the 4.8^2 nets is different from that of loomisite. The framework of hurlbutite belongs to the paracelsian-type structure, not the zeolite **ABW**-type.

Acknowledgements. We are grateful for the constructive comments by Structures Editor Peter Leverett and two anonymous reviewers, and help from Dr. Aaron Celestian and Dr. Anthony Kampf for identifying zeolite types. This study was funded by the Feinglos family and Mr. Michael Scott.

Supplementary material. To view supplementary material for this article, please visit https://doi.org/10.1180/mgm.2022.117

Competing interests. The authors declare none.

References

Brese N.E. and O'Keeffe M. (1991) Bond-valence parameters for solids. *Acta Crystallographica*, **B47**, 192–197.

Bu X., Feng P., Gier T.E. and Stucky G.D. (1997) Structural and chemical studies of zeolite ABW type phases: Syntheses and characterizations of an ammonium zincophosphate and an ammonium beryllophosphate zeolite ABW structure. *Zeolites*, **19**, 200–208.

Campbell T.J. and Roberts W.L. (1985) Mineral Localities in the Black Hills of South Dakota. *Rocks & Minerals*, **60**, 109–118.

Dal Bo F., Hatert F. and Baijot M. (2014) Crystal chemistry of synthetic $M^{2+}Be_2P_2O_8$ (M^{2+} = Ca, Sr, Pb, Ba) beryllophosphates. *The Canadian Mineralogist*, **52**, 337–350.

Frost R.L., Xi Y., Scholz R., Belotti F.M. and Filho M.C. (2012) Raman and infrared spectroscopic characterization of beryllonite, a sodium and beryllium phosphate mineral – implications for mineral collectors. *Spectrochimica Acta*, **A97**, 1058–1062.

Frost R.L., Scholz R., Lopez A., Xi Y., Queiroz C.S., Belotti F.M. and Filho M.C. (2014) Raman, infrared and near-infrared spectroscopic characterization of the herderite-hydroxylherderite mineral series. *Spectrochimica Acta*, **A118**, 430–437.

Gatta G.D., Jacobsen S.D., Vignola P., McIntyre G.J., Guastella G. and Abate L.F. (2014) Single-crystal neutron diffraction and Raman spectroscopic study of hydroxylherderite, $CaBePO_4(OH,F)$. *Mineralogical Magazine*, **78**, 723–737.

Grice J.D., Peacor D.R., Robinson G.W., Van Velthuizen J., Roberts W.L., Campbell T.J. and Dunn P.J. (1985) Tiptopite $(Li,K,Na,Ca,\square)_8Be_6(PO_4)_6(OH)_4$, a new mineral species from the Black Hills, South Dakota. *The Canadian Mineralogist*, **23**, 43–46.

Hatert F., Dal Bo F., Bruni Y., Meisser N., Vignola P., Risplendente A., Châtenet F.X. and Lebocey J. (2020) Limousinite, $BaCa[Be_4P_4O_{16}]\cdot 6H_2O$, a new beryllophosphate mineral with a phillipsite-type framework. *The Canadian Mineralogist*, **58**, 815–827.

Hawthorne F.C. and Huminicki D. (2002) The crystal chemistry of beryllium. Pp. 333–403 in: *Beryllium: Mineralogy, Petrology, and Geochemistry* (E.S. Grew, editor). Reviews in Mineralogy and Geochemistry, **50**. Mineralogical Society of America and the Geochemical Society, Chantilly, Virginia, USA.

Holland T.J.B. and Redfern S.A.T. (1997) Unit cell refinement from powder diffraction data: the use of regression diagnostics. *Mineralogical Magazine*, **61**, 65–77.

Kahlenberg V., Fischer R.X. and Baur W.H. (2001) Symmetry and structural relationships among ABW-type materials. *Zeitschrift für Kristallographie*, **216**, 489–494.

Kampf A.R. (1977) A new mineral: perloffite, the Fe^{3+} analogue of bjarebyite. *The Mineralogical Record*, **8**, 112–114.

Kampf A.R. (1992) Beryllophosphate chains in the structure of fransoletite, parafransoletite, and ehrleite and some general comments on beryllophosphate linkages. *American Mineralogist*, **77**, 848–856.

Libowitzky E. (1999) Correlation of O-H stretching frequencies and O–H···O hydrogen bond lengths in minerals. *Monatshefte für Chemie*, **130**, 1047–1059.

Lindbloom J.T., Gibbs G.V. and Ribbe P.H. (1974) The crystal structure of hurlbutite: A comparison with danburite and anorthite. *American Mineralogist*, **59**, 1267–1271.

Mandarino J.A. (1981) The Gladstone-Dale relationship: Part IV. The compatibility concept and its application. *The Canadian Mineralogist*, **19**, 441–450.

Moore P.B., Araki T., Kampf A.R. and Steele I.M. (1976) Olmsteadite, $K_2Fe_2^{2+}[Fe_2^{2+}(Nb,Ta)_2^{5+}O_4(H_2O)_4(PO_4)_4]$, a new species, its crystal structure and relation to vauxite and montgomeryite. *American Mineralogist*, **61**, 5–11.

Norton J.J. (1964) Pegmatites and other Precambrian Rocks in the Southern Black Hills; Geology and mineral deposits of some pegmatites in the southern Black Hills, South Dakota. *Geological Survey Professional Paper*, 297E. USGS Geological Survey. Washington, DC.

Ritz C., Essene E.J. and Peacor D.R. (1974) Metavivianite, $Fe_3(PO_4)_2\cdot 8H_2O$, a new mineral. *American Mineralogist*, **59**, 896–899.

Roberts W.L. and Rapp G. (1965) Mineralogy of the Black Hills. *South Dakota School of Mines and Technology (SDSMT)*, Bulletin 18. Dakota School of Mines, Dakota, USA.

Rouse R.C., Peacor D.R., Dunn P.J., Campbell T.J., Roberts W.L., Wicks F.J. and Newbury D. (1987) Pahasapaite, a beryllophosphate zeolite related to synthetic zeolite rho, from the Tip Top pegmatite of South Dakota. *Neues Jahrbuch für Mineralogie, Monatshefte*, **1987**, 433–440.

Sheldrick G.M. (2015a) SHELXT – Integrated space-group and crystal structure determination. *Acta Crystallographica*, **A71**, 3–8.

Sheldrick G.M. (2015b) Crystal structure refinement with SHELX. *Acta Crystallographica*, **C71**, 3–8.

Xing S., Luo M., Ni Yuan N., Liu D., Yang Y., Dai X., Zhang W. and Chen N. (2021) Accurate determination of plutonium in soil by tandem quadrupole ICP-MS with different sample preparation methods. *Atomic Spectroscopy*, **42**, 62–70.

Yang H., Gu X., Gibbs R.B. and Scott M.M. (2022) Loomisite, IMA 2022-003. CNMNC Newsletter 67. *Mineralogical Magazine*, **86**, https://doi.org/10.1180/mgm.2022.56

Zhang H., Chen M., Shi Z., Bu X., Zhou Y., Xu X. and Zhao D. (2001) Hydrothermal synthesis of new pure beryllophosphate molecular sieve phases from concentrated amines. *Chemical Materials*, **13**, 2042–2048.